ORIGINAL ARTICLE

M Dalstra
PM Cattaneo
F Beckmann

Synchrotron radiation-based microtomography of alveolar support tissues

Authors' affiliations:
M. Dalstra, P.M. Cattaneo, Department of Orthodontics, School of Dentistry, University of Aarhus, Denmark
F. Beckmann, Institute of Materials Research, GKSS Research Center, Geesthacht, Germany

Correspondence to:
Michel Dalstra, PhD
Department of Orthodontics
School of Dentistry
University of Aarhus
Vennelyst Boulevard 9
8000 Aarhus C
Denmark
Tel.: +45 8942 4190
Fax: +45 8619 2752
E-mail: mdalstra@odont.au.dk

Dates:
Accepted 11 September 2006

To cite this article:
Orthod Craniofacial Res **9**, 2006; 199–205
Dalstra M, Cattaneo PM, Beckmann F: Synchrotron radiation-based microtomography of alveolar support tissues

Structured Abstract

Authors – Dalstra M, Cattaneo PM, Beckmann F

Objectives – To study the alveolar support structures using synchrotron radiation (SR)-based microtomography with particular focus on the alveolar surface.

Design – High-resolution microtomography of jaw segments of various species and subsequent three-dimensional (3D) reconstruction.

Setting and Sample Population – Microtomography was performed at the DORIS-ring of the synchrotron facility of HASYLAB/DESY in Hamburg, Germany. The samples consisted of human, simian and porcine jaw segments.

Results – With SR being monochromatic, no beam-hardening artifacts could occur and the grey values in the scans were therefore directly related to the local tissue densities. Apart from the mineralized tissues, the beam energy was low enough to allow for the visualization of soft tissues like the fibers of the periodontal ligament (PDL) and blood vessels. 3D reconstructions of the alveolar bone showed that it can be rough and sharply edged. Furthermore, an intricate network of marrow cavities and blood vessels penetrates its surface. Differences in the local grey value distribution in the alveolar bone pointed to remodeling activity in the close vicinity of the PDL.

Conclusion – The assumption that the alveolar bone surface is smooth and continuous is not correct. This means that even small orthodontic loads can already give rise to high local stresses and strains in the bone and thus initiate remodeling processes.

Key words: dental alveolus, periodontal ligament, X-ray tomography

Introduction

In recent years, new radiographic imaging techniques have become available to the orthodontic community (1). Dental tomography, which was initially the exclusive playground of implantology and maxillofacial surgery, has gradually found its way to orthodontics and promises to have a great potential for diagnosis (2), examination (3) and treatment planning (4). Microtomography is another imaging modality which has recently been discovered for the orthodontic field. Verna and coworkers used microtomography to determine the type of tooth movement in a rat model (5,6), while the same group used 3D reconstructions of micro-CT scans to support their experimental findings of microcracks in porcine alveolar bone following orthodontic treatment (7). Microtomography has also been used to study bone reactions around implants used as orthodontic anchorage (8,9). Finally, it is also being used as a means to provide accurate geometrical data as input for finite element models of teeth and their supporting tissues (10,11).

In contrast to dental tomography, microtomography cannot be used on patients. Due to the limited size of the samples (the first medical microtomography systems were developed to examine trabecular bone biopsies), only excised samples of dental tissue can be scanned. However, as the samples due to their small size can come very close to the detector, the resolution for microtomography is typically in the range from 10 to 30 μm. Using synchrotron radiation (SR) as the X-ray source, this resolution can be brought even further down to the 1 μm range and below (12). Another advantage of using SR is its high brilliance. Even after monochromatizing the incident white beam there is enough intensity left to penetrate the sample. Radiation from a conventional X-ray source causes beam hardening, which means that the radiation from the low energy part of the spectrum becomes relatively more absorbed in the tissue then the radiation from high energy part. This makes that the grey values in the reconstructed images do not necessarily reflect the actual local attenuation coefficients of the tissue, which is usually expressed by the inner part of large slabs of tissue tending to become darker than it actually should be. As the incident beam is monochromatic for a synchrotron X-ray source the beam hardening effect does not occur, which means that the grey values are a direct reflection of the local attenuation coefficient, and thereby of the local density. The overall feature of SR-based microtomography is the excellent image quality of the 3D reconstructions though. Seeing meso- and microscopical anatomical features in three dimensions provides insights in their shape and functionality, which cannot be obtained from conventional 2D histology.

Having first used SR-based microtomography to study the osteonal organization in cortical bone, the authors have shown that it is possible to visualize and quantify the non-mineralized structures in bone like the network of haversian canals and the osteocyte lacunae (13). Consequently, a question came up whether something similar could be done for teeth and their alveolar support tissues, like the periodontal ligament (PDL). From an orthodontic point of view, this could perhaps provide answers as to why at present there seems to be a trend in clinical practice towards the use of lower forces necessary to move teeth (14). In order to fully comprehend the mechanics of the load transfer from teeth to the surrounding alveolar tissues during orthodontic treatment, it is important to know both shape and size of the tissues involved, as well as their material properties. It is common practice to estimate the pressure exerted onto the alveolar bone due to an orthodontic loading regime by dividing the applied force by an average value of the surface area of the alveolus of the considered tooth. The fact that in doing so, one inherently assumes the alveolus to be smooth and continuous is often forgotten though. The validity of this assumption is therefore scrutinized in this study, by performing ultrahigh-resolution micro-CT scans of the alveolar support tissues. In a broader sense, it was the aim of this study to examine whether SR-based microtomography can provide new insights into our present understanding of the structure and function of alveolar support tissues.

Materials and method

Various samples of the root/PDL/alveolar bone complex from human, simian and porcine origin were available for this study. The human sample was a segment of the mandible with the canine, two pre-molars and the first molar from a 19-year-old male donor obtained at autopsy. Five simian samples consisted of maxillary and mandibular segments, all containing a part of the canine,

a dental implant in the premolar region and the first molar from 6 to 7-year-old macaca fascicularis monkeys. The implants had been orthodontically loaded using either the canine or the first molar as anchorage to study the load transfer and tissue reaction of the surrounding bone (15). The porcine sample consisted of a single mandibular molar with the surrounding bone from a 3-month-old Danish landrace pig. This sample originated from an animal, which had been part of a study in which the presence of microcracks in the alveolar bone after orthodontic treatment was examined (7).

Before the scanning procedure, all samples had been fixated in 70% alcohol after excision. Subsequently, they were dehydrated in 96 and 99% alcohol and finally in an equal solution of 99% alcohol and acetone for 4 days each, after which they were embedded in methylmetacrylate. For this purpose, the human and simian samples had had the upper part of the crowns removed to keep the volume to be embedded to a minimum. It should be noted here that this particular specimen preparation procedure was performed to be able to cut histological slices of the samples after the microtomography scanning would have been finished and as such was not a prerequisite for the scanning itself.

The samples were scanned with a SR-based microtomograph operating in absorption mode (12). The experiments were conducted at the wiggler beamlines BW2 and W2 of the DORIS III-ring at HASYLAB/DESY in Hamburg, Germany. The two beamlines differ from one another with regard to the photon energy range (BW2: 8–24 keV; W2: 20–60 keV), beam size (BW2: 10×3.5 mm^2; W2: 15×4 mm^2) and best obtainable spatial resolution (BW2: 2 μm; W2: 3 μm). A double crystal Si(111) monochromator was used to monochromatize the incident white beam. After entering the X-ray detector, the monochromatic beam was converted by a fluorescent screen ($CdWO_4$, 500 μm thick) into visible light, which was then projected on the CCD camera (Apogee KX2, Kodak KAF 1600, 1536×1024 pixels, pixel length 9 μm Apogee Instruments Inc., Roseville, CA, USA) (Fig. 1).

The porcine sample was scanned at beamline BW2 at a photon energy of 24 keV and a pixel size of 3.8 μm. The sample holder rotated from 0 to 180° in steps of 0.25°, whereby the rotation centre was located in the middle of the CCD readout area. Being significantly larger, the human and simian samples were scanned at beamline W2, which allows for higher photon energies.

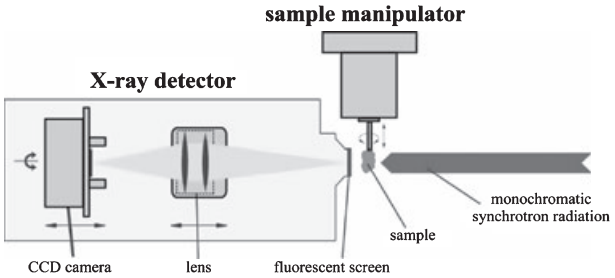

Fig. 1. Schematic overview of the scanning set-up.

The human sample was scanned there at a photon energy of 45 keV; the simian samples even slightly higher at 50 keV, due to the presence of the dental implant. For the human and simian samples, the pixel size was 16.4 μm. As the width of these samples exceeded the readout area of the CCD camera by almost a factor 2, the sample holder in these cases had to rotate from −180 to 180° in steps of 0.25° to acquire the full image, this time with the rotation centre located to the side of the CCD readout area. The two by 180° shifted projection images were finally digitally combined into a complete projection image of almost the double CCD width.

The single-slice reconstructions were calculated from the raw data (sinograms) with a filtered back-projection algorithm using IDL software (Research Systems Inc., Boulder, CO, USA). These images were then subsequently stacked to create a three-dimensional (3D) voxel data set. Due to the limited size of the beam, the long samples had to be scanned at different, slightly overlapping heights. Afterwards the data sets of the individual heights were then merged to create the data sets of the entire samples using special 3D visualization software (VG Studio, Volume Graphics GmbH, Heidelberg, Germany).

Results

Human sample

Transverse sections through the mandible revealed that the alveolar bone proper was quite thin. Especially, in the apical region the lamina dura was not much thicker than the PDL (Fig. 2). Perforations of the socket appeared to be most frequent in the cervical region. The circumferential organization of the haversian network in the outer wall of the mandible was clearly visible (Fig. 3).

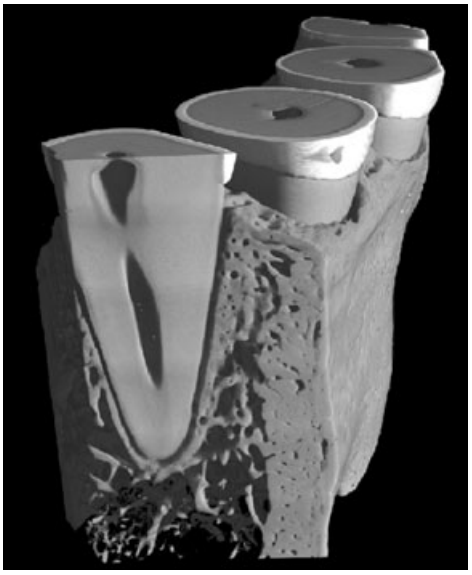

Fig. 2. View through the 3D reconstruction of the entire segment of a human mandible with three transverse single-slice images. Note the decreasing density of the alveolar bone going from cervical to apical level of the roots.

The longitudinal cuts through the 3D reconstruction showed how the sockets appeared to be only sparsely suspended by a few trabeculae. In the mesiodistal aspect, it could clearly be observed that this degree of support decreased steadily from cervical towards apical level. Moreover, in the buccolingual aspect the support of the alveolar bone proper was inhomogeneous due to the immediate presence of the buccal mandibular cortex (Fig. 4).

Simian samples

The alveolar tissues in the simian samples had been exposed to severe biological interference due to the placement of the dental implant and its subsequent exposure to the orthodontic loading regime. As a result ample evidence of the tissue reactions was encountered: new bone formation occurred in the bucco-apical and bifurcation regions of the alveolus of the premolar (Fig. 5) and areas of severe root resorption were observed on the canine (Figs 5 and 6).

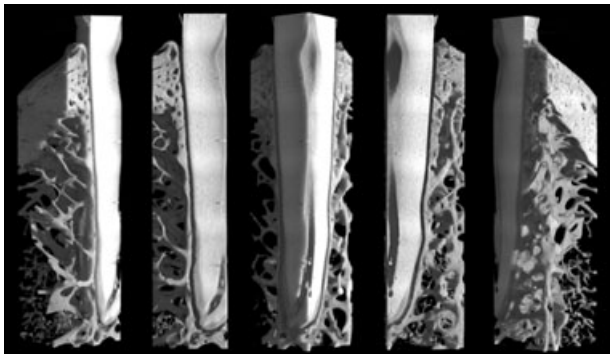

Fig. 3. Five views of the buccal quarter of the second premolar with its surrounding bone. Distal view on the left; lingual view in the middle and mesial view on the right with the respective quarter views in between.

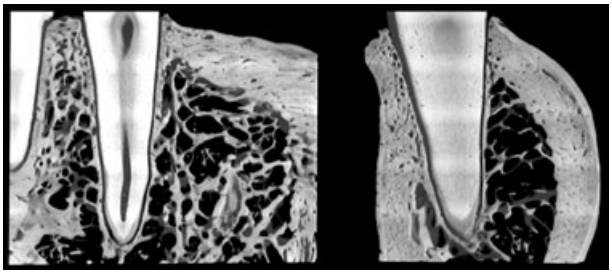

Fig. 4. Mesiodistal (left) and buccolingual (right) views of the alveolus of the canine. Note the uneven thickness of the alveolar bone proper and the sparse trabecular support.

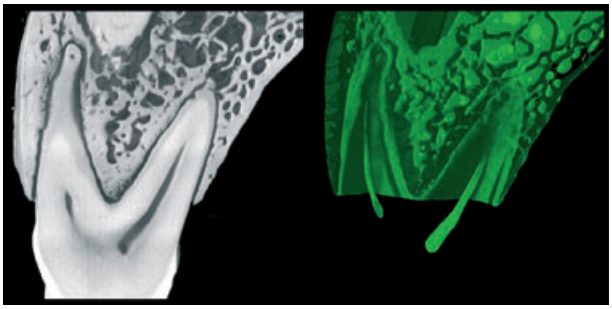

Fig. 5. Buccolingual view through the 3D reconstruction of the segment of one of the simian maxilla at the level of the first premolar (left). False-coloring is used to visualize the non-mineralized tissues and structures, like the root canals, PDL and bone marrow (right). Note the areas of new bone formation around the apex of the buccal root and at the bifurcation.

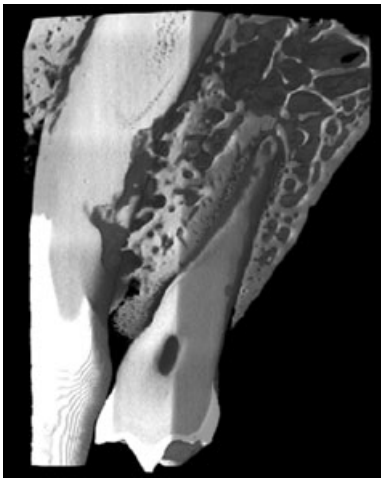

Fig. 6. Close-up view of the extensive amount of root resorption taking place on the distal surface of the large root of the canine.

Porcine sample

Due to the higher resolution, the amount of detail in the porcine sample was much larger than for the human and simian samples. The alveolar bone surface was very rough and although the trabecular bone was very dense, no lamina dura was evident (Fig. 7). On the side of the root, the interface between dentine and cementum was clearly visible due to the higher porosity and slightly lower degree of mineralization of the latter. By using false-coloring features within the non-mineralized phase could be enhanced. By digitally removing the mineralized tissues, an image could be formed of the marrow space, blood vessels and the PDL (Fig. 8). On the root/PDL interface the Sharpey's fibers could be seen to extend radially from the PDL into the cementum layer. The PDL/bone interface had a more open character where a myriad of blood vessels crossed between bone marrow and PDL. Inside the PDL itself, the radial orientation of the ligament fibers could also be distinguished.

Discussion

Different examples of the tooth/PDL/alveolar bone complex from various species (human, simian and porcine) have been scanned using ultrahigh-resolution SR-based microtomography. The material was collected piecewise from other studies at the Department of Orthodontics, University of Aarhus, Denmark. For the actual selection of this material a balance had to be struck between having a broad range of samples to visualize and examine different anatomical features of the alveolar support tissues on the one hand, and the limited amount of beam time to perform the scannings at the SR facility on the other. As such this study explores the use of SR-based microtomography as a new imaging method in the dental/orthodontic field. Due to the small sample size, no individual variations could be taken into account.

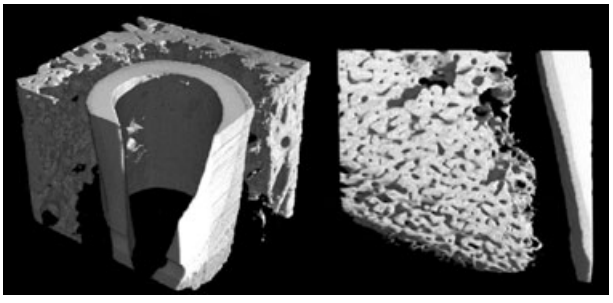

Fig. 7. The mineralized tissues in 3D reconstructions of the entire porcine sample (left) and of a longitudinal section through the alveolus (right). Note the absence of a clear lamina dura.

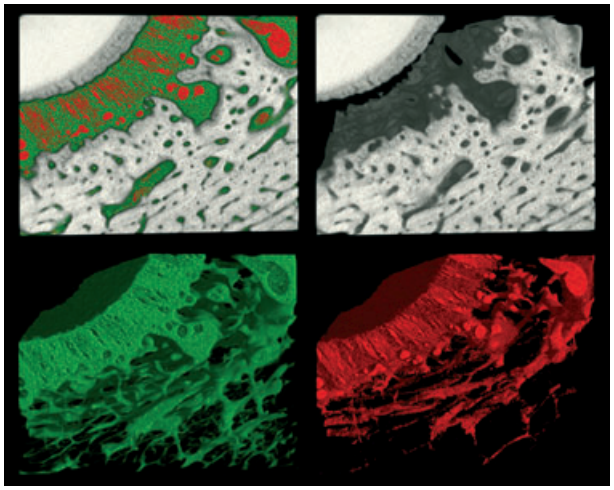

Fig. 8. 3D reconstruction of the mineralized and soft tissues in a section of the porcine sample. Note the use of false-coloring to enhance the low-density structures; green for the bone marrow and the fibers of the PDL; red for the blood vessels and interstitial tissue.

The SR-based microtomography images of the jaw segments presented in this study give rise to a new appraisal of the structure and architecture of the alveolar support tissues. The combination of ultrahigh resolution and the monochromatic radiation yield an image quality, which cannot be rivaled with conventional microtomography (8). The picture of the anatomy of the alveolar support tissues that most dentists have in their mind is based on conventional histological slices and/or anatomical drawings. It can, however, be difficult to mentally extrapolate these 2D images to the third dimension.

Being confronted with the delicate shape of alveolar sockets in the human segment and their sparse trabecular support makes one suddenly realize that not much loading of the teeth would be necessary to start deforming the alveolar bone noticeably. In the orthodontic field, there is an on-going tendency towards the use of smaller loads to move teeth. There is experimental and clinical evidence that teeth can already be moved with forces as low as 10 cN (16–18). Looking at the bony surfaces of the alveoli in the various samples, it is not exactly smooth and continuous. Unlike the outer surface of the root, the surface of the alveolar bone is rough and uneven. An extreme case is

presented by the porcine alveolus, where radially orientated bony spiculae point toward the root. This is not the case for the human and simian samples, yet these display various degrees of porosity of the lamina dura. This means that the internal stresses in the alveolar bone due to orthodontic loading are not just determined by dividing the orthodontic load by the cross-sectional surface area of the alveolus. As the actual cross-sectional surface area is reduced due to this porosity, the real stress levels will consequently be higher. This means that even small orthodontic loads could already give rise to high local stresses and strains in the bone and thus initiate remodeling processes.

The inhomogeneous and asymmetric nature of the alveolus and its bony support has also consequences for the exact location of the center of resistance (CR) of the tooth. In the past, holographic analyses have revealed discrepancies between experimental and theoretical locations of the CR along the longitudinal axis of the root (19), which can be attributed to this non-uniform alveolar support. However, the asymmetric alveolar support in the buccolingual direction with the thick outer cortex on the buccal side directly next to the PDL and the considerably looser trabecular support on the lingual side must also lead to a deviation from the longitudinal axis of the root in this aspect. The exact location, which apart from the anatomical geometry is also dependent on the non-linear material behavior of the PDL, can be determined using highly detailed finite element models based on the microtomography data (20).

Using false-coloring to visualize the non-mineralized tissues has revealed that the PDL cannot be considered as an isolated organ. The intricate network of blood vessels cutting through the lamina dura and thus forming connections between the PDL and the bone marrow surrounding the socket is evidence for a close biological and mechanical interaction between these two tissues. Although it is still unknown, whether orthodontically induced bone remodeling is initiated by mechanical stimuli inside the PDL or the alveolar bone (21), the anatomical infrastructure is present for an exchange of these stimuli between PDL and alveolar bone.

The monochromatic radiation used for SR-based microtomography makes that the grey values in the reconstructed images are directly related to the local degree of mineralization (13, 22–24). For the samples presented in this study, this not only meant that different mineralized tissues with various degrees of mineralization (bone, dentine, cementum and enamel) could be visually identified, but that areas of bone formation, where the new bone is still less mineralized, could be visualized as well. In the cortical walls of the human and simian samples, this could be observed as slightly darker osteons, while the simian and porcine samples also presented new bone formation in the form of less mineralized and more porous bone in the close vicinity of the PDL. In the simian samples, this probably occurred as the affected tooth (first pre-molar) was pushed against by the orthodontically loaded canine, while in the porcine sample the bone formation was rather part of the physiological growth of the animal as this particular tooth had not been subject to orthodontic loading.

Conclusions

(1) Microtomography of alveolar support tissues provides new insights in and appreciation of their 3D structure and architecture.
(2) The delicate network of alveolar bone supporting the teeth can explain the rationale for the current tendency towards the use of lower forces in orthodontic treatment.
(3) The support of the alveolar bone is non-uniform, which means that it can be anticipated that functional and/or orthodontic load transfer from the teeth to the surrounding bone is non-uniform too.
(4) The location of the center of resistance of a tooth can only be determined approximately; its exact position is influenced by the non-uniform load transfer.

Acknowledgements: This work has been financially supported by the European Commission (IHP-contracts II-00-064 EC and II-03-052 EC).

References

1. Quintero JC, Trosien A, Hatcher D, Kapila S. Craniofacial imaging in orthodontics: historical perspective, current status, and future developments. *Angle Orthod* 1999;**69**:491–506.
2. Hatcher DC, Aboudara CL. Diagnosis goes digital. *Am J Orthod Dentofacial Orthop* 2004;**125**:512–5.

3. Gunduz E, Rodriguez-Torres C, Gahleitner A, Heissenberger G, Bantleon HP. Bone regeneration by bodily tooth movement: dental computed tomography examination of a patient. *Am J Orthod Dentofacial Orthop* 2004;**125**:100–6.
4. Huang J, Bumann A, Mah J. Three-dimensional radiographic analysis in orthodontics. *J Clin Orthod* 2005;**39**:421–8.
5. Verna C, Dalstra M, Melsen B. The rate and the type of orthodontic tooth movement is influenced by bone turnover in a rat model. *Eur J Orthod* 2000;**22**:343–52.
6. Verna C, Dalstra M, Melsen B. Bone turnover rate in rats does not influence root resorption induced by orthodontic treatment. *Eur J Orthod* 2003;**25**:359–63.
7. Verna C, Dalstra M, Lee TC, Cattaneo PM, Melsen B. Microcracks in the alveolar bone following orthodontic tooth movement: a morphological and morphometric study. *Eur J Orthod* 2004;**26**:459–67.
8. Cattaneo PM, Dalstra M, Beckmann F, Donath T, Melsen B. Comparison of conventional and synchrotron radiation-based microtomography of bone around dental implants. In: Bonse U, editor. *Developments in X-Ray Tomography IV, Proceedings of SPIE*, Vol. 5535. Bellingham, WA: SPIE, 2004, pp. 757–64.
9. Yip G, Schneider P, Roberts EW. Micro-computed tomography: high resolution imaging of bone and implants in three dimensions. *Sem Orthod* 2004;**10**:174–87.
10. Cattaneo PM, Dalstra M, Melsen B. The finite element method: a tool to study orthodontic tool movement. *J Dent Res* 2005;**84**: 428–33.
11. Rahimi A, Keilig L, Bendels G, Klein R, Buzug TM, Abdelgader I et al. 3D reconstruction of dental specimens from 2D histological images and microCT-scans. *Comput Methods Biomech Biomed Engin* 2005;**8**:167–76.
12. Bonse U, Busch F, Günnewig O, Beckmann F, Pahl R, Delling G et al. 3D computed X-ray tomography of human cancellous bone at 8 microns spatial and 10^{-4} energy resolution. *Bone Miner* 1994;**25**:25–38.
13. Dalstra M, Karaj E, Beckmann F, Andersen T, Cattaneo PM. Osteonal mineralization patterns in cortical bone studied by synchrotron radiation-Based computed microtomography and scanning acoustic microscopy. In: Bonse U, editor. *Developments in X-Ray Tomography IV, Proceedings of SPIE*, Vol. 5535. Bellingham, WA: SPIE, 2004, pp. 143–51.
14. Ren Y, Maltha JC, Kuijpers-Jagtman AM. Optimum force magnitude for orthodontic tooth movement: a systematic literature review. *Angle Orthod* 2003;**73**:86–92.
15. Cattaneo PM, Dalstra M, Beckmann F, Donath T, Melsen B. Analysis of stress and strain around orthodontically loaded implants: an animal study. *International J Oral Maxillofac Implants* 2006;**21**: in press.
16. van Leeuwen EJ, Maltha JC, Kuijpers-Jagtman AM. Tooth movement with light continuous and discontinuous forces in beagle dogs. *Eur J Oral Sci* 1999;**107**:468–74.
17. Iwasaki LR, Haack JE, Nickel JC, Morton J. Human tooth movement in response to continuous stress of low magnitude. *Am J Orthod Dentofacial Orthop* 2000;**117**:175–83.
18. van't Leeuwen EJ, Maltha JC, Kuijpers-Jagtman AM, van Hoff MA. The effect of retention on orthodontic relapse after the use of small continuous or discontinuous forces. An experimental study in beagle dogs. *Eur J Oral Sci* 2003;**111**:111–6.
19. Burstone CJ, Pryputniewicz RJ. Holographic determination of centers of rotation produced by orthodontic forces. *Am J Orthod* 1980;**77**:396–409.
20. Cattaneo PM, Dalstra M, Melsen B. Moment-to-force ratio, center of rotation and force level: a finite element study predicting their interdependency for simulated orthodontic loading regimes. *Am J Orthod Dentofacial Orthop* 2006;**130**:in press.
21. Bourauel C, Vollmer D, Jäger A. Application of bone remodeling theories in the simulation of orthodontic tooth movements. *J Orofac Orthop* 2000;**61**:266–79.
22. Dowker SEP, Elliot JC, Davis GR, Wilson RM, Cloetens P. Synchrotron x-ray microtomographic investigation of mineral concentrations at micrometre scale in sound and carious enamel. *Caries Res* 2004;**38**:514–22.
23. Kinney JH, Nalla RK, Pople JA, Breunig TM, Ritchie RO. Age-related transparent root dentin: mineral concentration, crystallite size, and mechanical properties. *Biomaterials* 2005;**26**:3363–76.
24. Prymak O, Tiemann H, Sötje I, Marxen JC, Klocke A, Kahl-Nieke B et al. Application of synchrotron-radiation-based computer microtomography (SRmuCT) to selected biominerals: embryonic snails, statoliths of medusae, and human teeth. *J Biol Inorg Chem* 2005;**27**:1–8.